

Influence of Niobium Pentoxide and Sintering Temperature on Mechanical and Electrical Properties of Glass-ceramics Obtained from Recycled Automotive Windshields

Hiasmim R. Gualberto^{a,b}, Kelly C. da Silveira^b, Fernanda A. N. G. da Silva^c, Marcio A. Sens^d,
Ivan N. Bastos^{b*} , Edgard Poiate Júnior^b, Mônica C. de Andrade^b

^aInstituto Federal Fluminense, Quissamã, RJ, Brasil.

^bUniversidade do Estado do Rio de Janeiro, Instituto Politécnico, Nova Friburgo, RJ, Brasil.

^cUniversidade Federal do Rio de Janeiro, Instituto de Química, Rio de Janeiro, RJ, Brasil.

^dUniversidade Federal Fluminense, Departamento de Engenharia Elétrica, Niterói, RJ, Brasil.

Received: November 04, 2021; Revised: April 25, 2022; Accepted: May 11, 2022

Automotive windshield represents a large volume of solid waste due to limited recycling. Glass-ceramics were produced from discarded windshields with Nb₂O₅ as a nucleating agent at concentrations of 0, 5, 10, and 15 wt% at 700 and 800 °C sintering temperatures. Mechanical and electrical characterizations of glass-ceramics were performed. Equibiaxial flexural strength was performed and related to porosity. At 700 °C, Nb₂O₅ favors the monoclinic NaNbO₃ phase with perovskite structure. At 800 °C, high Nb₂O₅ content formed crystalline phases of perovskite and quartz. Dielectric constant and electrical conductivity increased with the addition of Nb₂O₅, reaching 64 and 4.3 μS/m for 15 wt% Nb₂O₅ at 700 °C. At 800 °C, niobium pentoxide reduces the biaxial flexural strength from 28.7 to 14.4 MPa; while increasing the electrical conductivity from 0.10 to 0.33 μS/m for samples with 0 and 15 wt%.

Keywords: *Recycled windshield, niobium pentoxide, flexural strength, electrical properties.*

1. Introduction

Environmental problems like the increasing number of landfills and depletion of natural resources are becoming more critical. Glass recycling is a well-known process; however, glass is one of the primary solid wastes in landfills. Moreover, the world car production reaches around 70 million units per year¹, and every car uses *ca.* 13 kg of glass², especially in the windshields. Therefore, the reuse and recycling of automotive windshields^{3,4} must be incentivized to reduce the environmental impacts. The development of new materials from solid waste can reduce the consumption of raw materials and energy^{4,5,6}.

Waste glass can be heat treated to produce glass-ceramics, which are materials with excellent mechanical properties, durability, biocompatibility, and chemical stability, presenting better properties than previous glass⁷. However, the properties are strongly influenced by the chemical composition of raw material and the processing routes, such as heat treatment^{7,8}. Thus, the applications are diverse, for example, porous glass-ceramics⁹ that absorb sound¹⁰, dense glass-ceramics for tiles of civil construction,^{11,12} or even biomedical ceramics applied to prostheses and teeth¹³.

The production of glass-ceramics from solid waste is an alternative to reduce the environmental impacts and the withdrawal of natural resources. Therefore, several residues have been used to obtain glass-ceramics with different characteristics and applications, as shown in the following cited works. Si and Ding¹⁴ produced wollastonite glass-

ceramics from window glass powder. Yan et al¹⁰ have produced porous glass-ceramics from high titanium blast furnace slag, and waste glass was applied to sound absorption. Similarly, Cao et al.¹⁵ produced porous glass-ceramics with metallurgical slag and glass residues. Yio et al.¹⁶ used furnace bottom ash and glass. Zhang and Liu¹⁷ produced glass-ceramics from soda-lime glass waste with suitable mechanical properties for civil structures. Kang et al.¹⁸ and Lu et al.⁵ used granite waste to produce glass-ceramics, and they evaluated the nucleating agent effects. Thus, the reuse of solid waste and the production of glass-ceramics has been investigated aiming at diverse applications, in a growing concern about the effects on climate change.

In the case of recycled glass to produce glass-ceramics, the raw materials can come from objects like bottles, soda-lime glass, photovoltaic glass, and liquid crystal display (LCD) glass¹⁹. In addition to these sources, automotive laminated glass has also been reused to produce new materials, despite being more challenging to recycle due to its mixture with polymer PVB - polyvinyl butyrol^{2,20}. Souza-Dal Bó et al.²¹ used laminated glass waste to manufacture ceramic frits used in floor and wall coatings. Waste produced by the automotive industry improves the mechanical properties of white ceramics²². Therefore, automotive laminated glass can be reused efficiently and economically, benefiting the environment.

Nucleating agents ease the crystallization of amorphous materials. Lu et al.²³ obtained an increase in crystallinity with higher concentrations of MgO in glass-ceramics from waste materials. Similarly, Lu et al.⁵ also obtained increased

*e-mail: inbastos@iprj.uerj.br

crystallinity in their glass-ceramics with different boehmite contents. Moreover, the nucleating agents significantly alter the glass-ceramic behavior after the sintering process, affecting the physical, chemical, and mechanical properties^{24,25}. For instance, Fan et al.¹⁹ analyzed the effects of magnesium oxide on the dielectric properties and flexural strength of glass-ceramics obtained from the glass of liquid crystal display (LCD).

Niobium pentoxide has attracted interest because it affects relevant properties of glasses and glass-ceramics; in these materials, niobium oxide can change density, dielectric constant²⁶, crystallinity^{27,28}, chemical stability¹³, and biocompatibility¹³. It is used as a nucleating agent^{27,29} to promote crystallization that influences the optical and dielectric properties of glass-ceramics³⁰. Moreover, improved chemical stability and biocompatibility by applying niobium oxide as a nucleating agent have been reported²⁹. Hence, great attention has been raised considering adopting of the niobium oxide as a nucleating agent for glass-ceramics in electronic and biomedical applications³⁰. Thus, it has been used in the products such as batteries, solar cells, supercapacitors, prostheses, and even as dental material^{31,32,33}. Nevertheless, as Zhao et al.²⁶ reported, the effects of this nucleating agent on the microstructure and properties of glass-ceramics are not yet clearly understood. In their work²⁶, the addition of niobium pentoxide increased the dielectric constant of glass-ceramics. This effect was related to the formation of the calcium pyroniobate phase, which has a dielectric constant higher than diopside that was the predominant phase in glass-ceramics produced without niobium oxide as nucleating agent. The authors reported that the enhanced crystallization caused by niobium pentoxide, at least for diopside glass-ceramics, has a mechanism different than those of traditionally nucleating agents such as Fe₂O₃, Cr₂O₃, and TiO₂. In previous work, Gualberto et al.³⁴ identified the formation of sodium niobate with the use of niobium pentoxide. The alkali niobates (K,Na)NbO₃, named KNN, have extremely good piezoelectric properties, although their synthesis is difficult and the crystalline structure complex²⁹.

In this work, we sought to investigate the production of glass-ceramic from automotive windshield glass, with the selection of niobium pentoxide as a nucleating agent. The characterization was carried out to evaluate the influence of the nucleating agent concentration and sintering temperature on the mechanical and electrical properties of the glass-ceramics produced from recycled windshields.

2. Materials and Methods

2.1. Production of glass-ceramics

The used windshield contained two layers of glass intercalated with a polymer layer of polyvinyl butyral (PVB). The glasses were obtained from scrapped cars (model Gol, carmaker Volkswagen, Brazil). The chemical

composition of the windshield glass is given in Table 1³⁴, and it was evaluated by quantitative x-ray fluorescence. This composition is compatible with float glass produced with silica-soda-lime, that are used in the windshields of different car brands³⁵. According to Saint-Gobain publication³⁶, the commercial original and spare windshields made from float glass have stringent specifications.

The used windshield glass was cut into smaller pieces and placed in the ball mill container along with the alumina grinding bodies. A ball mill with a diameter of 170 mm and a length of 230 mm was used. Three types of spheric bodies were used. They had diameters of 40, 35, and 25 mm, and the quantity of each body type was 15, 30, and 90 balls, respectively. A mass of 1.0 kg of the dry windshield was used. Dry grinding was carried out for 24 h with a 100-rpm rotation.

After this process, the larger pieces of glass and PVB were manually separated and removed from the produced glass powder. The glass powder had its particles classified through a 65-mesh sieve. The specimens were molded with four concentrations of Nb₂O₅ (CBMM, Brazil, purity higher than 98.5%) added to the glass powder. The final composition of specimens had 0, 5, 10, and 15 wt% of niobium pentoxide.

During the forming process, pure water was added (10 wt%) to facilitate the compaction of samples. Samples of 3.0 g were compacted in a circular metal die, with a diameter of 24.0 mm, applying a uniaxial pressure of 25.8 MPa for one minute (P10 ST, 98 kN hydraulic press, Bovenau, Brazil). The shaped specimens were dried in an oven (400/3ND, New Ethics, Brazil) at 110 °C for 1.0 h. Subsequently, the samples were sintered in a muffle furnace (N1100, Fornitec, Brazil) with a heating rate of 5.0 °C/min at the final temperatures of 700 or 800 °C for 1.0 h. Based on works in which glass-ceramics were produced from raw materials similar to the windshield glass^{5,15,19,23,26}, the adopted sintering temperatures were 700 and 800 °C. These temperatures were probably higher than glass transition temperature (T_g) and close to the crystallization temperature (T_c). Therefore, a lower heating rate was used to allow good densification before the crystallization onset. The chosen 1.0 h sintering time is based on past experiences³⁷, comparing glass-ceramics obtained from 1.0 h to 3.0 h sintering times.

The adopted sintering time resulted in a denser glass-ceramic than those sintered for 3.0 h, being 1.0 h preferred in this study. Four compositions and two sintering temperatures were used; thus, eight groups were produced. The L group is related to samples sintered at 700 °C and the H to those sintered at 800 °C. The numbers 0, 5, 10, and 15 wt% are related to the amount of niobium pentoxide added. For each test, at least 10 samples were prepared and tested.

2.2. Characterization

Differential thermal analysis (DTA) of the green bodies was performed in the Simultaneous Thermal Analyzer STA 6000 (PerkinElmer, USA). The tests were carried out

Table 1. Glass composition of windshield.

Composition	SiO ₂	Na ₂ O	CaO	MgO	Al ₂ O ₃
Wt. (%)	80.10	8.86	7.97	2.34	0.73

in an air atmosphere, with a heating rate of 5.0 °C/min, the same as the sintering process, starting from 30 to 900 °C.

X-ray diffraction (XRD) was performed in a milled sample of each group after sintering. The powder method was selected, with CuK α radiation, at 40 kV/40 mA, goniometer speed of 0.02° per step, with a count time of 0.5 s per step, being 2 θ collected from 5 to 75°, with position-sensitive detector (LynxEye, England). Qualitative interpretations of the spectra were performed by comparison with standards of the PDF02 database (The ICDDs Powder Diffraction File™, PDF®).

The bulk specific mass, the apparent porosity, and the water absorption were obtained according to Archimedes' method. Ten specimens were used for each experimental condition studied.

The biaxial flexural strength test was conducted on a universal testing machine AGX-Plus (Shimadzu, Japan), following the standard test method C1499-15 for monotonic equibiaxial flexural strength of advanced ceramics at ambient temperature³⁸. Following the standard, ten specimens were tested to obtain the average of each group. This test is ring-on-ring type, where the uniaxial load is applied by a ring in the center of the specimen, and another ring supports the specimens. Masking tape was used to keep the fragments of the specimen together after the fracture. The breaking biaxial stress supported by the specimen, σ_f , is obtained by Equation (1).

$$\sigma_f = \frac{3F}{2\pi h^2} \left[(1-\nu) \frac{D_S^2 - D_L^2}{D^2} + (1-\nu) \ln \left(\frac{D_S}{D_L} \right) \right] \quad (1)$$

The parameter D_S is the mean diameter of the outer ring that supports the specimen. D_L is the mean diameter of the inner ring that loads the specimen. D is the average of three measurements of the diameters, and h is the average of three thickness measurements. F is the breaking load supported by the specimens. The parameter ν is the glass-ceramic Poisson coefficient (0.20)³⁹. The samples break within 10-15 s under an average displacement rate of 0.50 mm/min. D_S and D_L diameters have values of 12.0 mm and 5.0 mm, respectively. Ten replicas were used to estimate the mechanical behavior for each condition. The reliability of the biaxial flexural strength results was determined by the Weibull method⁴⁰. Moreover, Tukey tests was applied to the flexural strength with 0.05 confidence level to reveal the influence of niobium pentoxide content.

The scanning electron microscopy (SEM) analysis was carried out on the fracture surface of the specimens. The microscope JSM-6510LV (JEOL, Japan) was used.

The dielectric properties were determined by applying a voltage of 1.0 V, varying the frequency from 20 Hz to 100 kHz; however, the parameters were taken at 1.0 kHz. The electrical measurement was performed with Wayne Kerr 3245 inductance analyzer (Wayne Kerr Electronics, UK). Additionally, the dissipation factor (k), which allows evaluating the electrical conductivity of the material (σ_{el}), was measured according to Equation (2).

$$\sigma_{el} = k\omega C \frac{L}{A} \quad (2)$$

where C is the capacitance of electrode, ω is the angular frequency, L is the length, and A is the cross-sectional area⁴¹.

Five specimens from each group were tested. This test used adhesive electrodes for electrostimulation (Carcitrode, Brazil) cut in the sample size. The electrodes were assembled as a sandwich, and the measurement of glass-ceramic properties was performed. A four-wire configuration was used to improve the accuracy by reducing the effects of Ohmic resistances of contacts and wires. The average cross-section area and the length were 380 mm² and 3.9 mm, respectively.

3. Results and Discussion

The differential thermal analysis (DTA) data are depicted in Figure 1. There is an inflection point with low intensity in the curves in the 600-700 °C range. This event is likely associated with the glass transition temperature, T_g. Zhao et al.²⁶ reported the T_g was close to 635 °C for glass-ceramics produced with vitreous materials of similar composition with Nb₂O₅ addition. Nonetheless, they also did not observe a significant influence of Nb₂O₅ on T_g. As the nucleation in glasses generally starts around 50 °C above the T_g^{26,42,43}, the sintering temperatures adopted for the glass-ceramics in this paper were probably higher than the T_g.

Figure 2 depicts the diffractograms of sintered glass-ceramics for 1.0 h at 700 and 800 °C for different niobium pentoxide contents. Crystalline phase peaks are identified in all glass-ceramics, except at 700 °C without Nb₂O₅, although not detected by DTA analysis, likely due to the short time in high temperature of thermal analysis. Zhao et al.²⁶ also identified the reduction in the crystallization temperature of glass-ceramics with the addition of this nucleating agent. In the present work, temperatures of 700 and 800 °C were used to sinter glass-ceramics, both higher than T_g, to crystallize the material with Nb₂O₅. According to Morais et al.⁴³, crystalline phases were found for pure Nb₂O₅ above 550 °C. Below 550 °C, the samples remain amorphous.

Different crystallization of XRD spectra were observed with Nb₂O₅ presence in 5, 10, and 15 wt%. At 700 °C, the formation of the NaNbO₃ monoclinic phase with perovskite (P) structure (JCPDS 01-074-2449 and 00-044-0060) was observed with characteristic peaks at 14.42, 17.18, 22.58, 28.35, 29.10, 29.59, 32.42, 36.58, and 46.25. In addition,

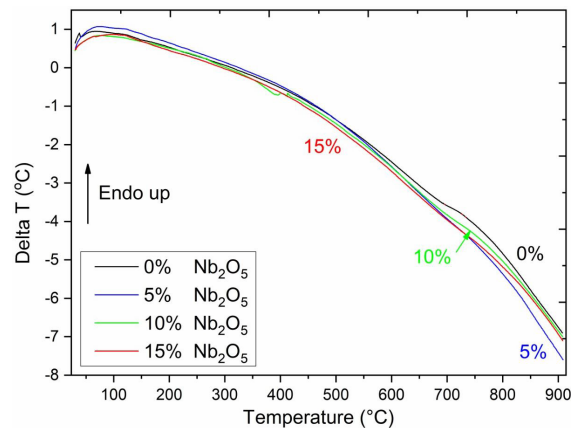


Figure 1. Differential thermal analysis curves of green bodies with and without the addition of Nb₂O₅ at concentrations of 0, 5, 10, and 15 wt%.

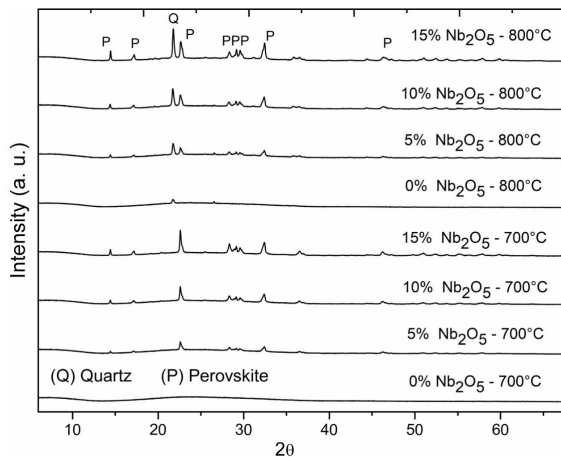


Figure 2. Diffractograms of sintered glass-ceramics for 1.0 h, at 700 and 800 °C for different niobium pentoxide contents.

peaks between 51.1 and 57.91 (2θ) were observed by Morais et al.⁴³ and Li et al.⁴⁴. The diffractograms for samples sintered at 800 °C showed the monoclinic formation of NaNbO_3 , the same phase observed in samples at 700 °C; however, the crystalline peak was associated with quartz (Q)^{45,46}.

The diffractograms of glass-ceramic produced at 800 °C reveal a peak at 21.74° related to the highest intensity peak of the crystalline structure of quartz (Q). Since the second-most intense peak is not identified at 35.67°, it suggests an imperfect structure. Furthermore, the peak at 21.74° is not observed at 700 °C. Thus, even without adding the nucleating agent, an incipient crystallization occurs at 800 °C but not at 700 °C.

Table 2 shows the sintered glass-ceramic average specific mass, porosity, and water absorption for 1.0 h at 700 and 800 °C. There is an increase in the values of apparent porosity with the concentration of niobium pentoxide at both temperatures. When comparing the sintering temperatures, it is observed that the specimens at 800 °C absorb less water and have lower apparent porosity, even though they are less dense. In this case, this may be due to greater surface glazing at 800 °C, which prevents water absorption. This vitrification does not occur in the sample bulk, as evidenced by SEM (Figure 3). This phenomenon hinders the water penetration in Archimedes' tests, also observed in the previous work³⁴.

Samples sintered at 800 °C exhibited a lower specific mass than those sintered at 700 °C, even with less apparent porosity and water absorption. Specific mass is influenced by the flow viscosity of the sintering materials. Viscous flow and crystallization increase at high temperatures; however, an intense crystallization before sintering produces a porous material^{8,19}. Thus, a higher temperature favors crystallization, hinders the sintering, and produces a lower specific mass. This fact is consistent with the higher porosity observed in the fracture surface of samples sintered at 800 °C (Figure 4).

At elevated temperatures, Zhang and Liu¹⁷ observed higher surface densification than in bulk. Moreover, at higher temperatures, the viscous flow resistance of glass is lower at the surface than in bulk. Thus, it is noticed that specimens sintered at 800 °C densified more intensely on the surface, resulting in lower water absorption and apparent porosity.

Table 2. Specific mass, porosity, and water absorption of sintered groups at 700 and 800 °C.

Group	Property	Mean \pm SD
L0	Specific mass (g/cm ³)	2.422 \pm 0.045
	Water absorption (%)	0.417 \pm 0.665
	Porosity (%)	0.998 \pm 0.562
L5	Specific mass (g/cm ³)	2.393 \pm 0.015
	Water absorption (%)	0.642 \pm 0.113
	Porosity (%)	1.547 \pm 0.273
L10	Specific mass (g/cm ³)	2.332 \pm 0.076
	Water absorption (%)	2.085 \pm 0.657
	Porosity (%)	4.945 \pm 1.467
L15	Specific mass (g/cm ³)	2.205 \pm 0.019
	Water absorption (%)	6.789 \pm 0.443
	Porosity (%)	16.055 \pm 0.998
H0	Specific mass (g/cm ³)	1.868 \pm 0.006
	Water absorption (%)	0.042 \pm 0.009
	Porosity (%)	0.079 \pm 0.017
H5	Specific mass (g/cm ³)	1.900 \pm 0.009
	Water absorption (%)	0.146 \pm 0.030
	Porosity (%)	0.278 \pm 0.058
H10	Specific mass (g/cm ³)	1.839 \pm 0.013
	Water absorption (%)	0.684 \pm 0.174
	Porosity (%)	1.267 \pm 0.322
H15	Specific mass (g/cm ³)	2.062 \pm 0.016
	Water absorption (%)	3.119 \pm 0.309
	Porosity (%)	6.639 \pm 0.663

Figures 3 and 4 show the SEM images of glass-ceramics sintered at 700 and 800 °C, respectively. The fracture surface of samples with 0, 5, 10, and 15 wt% of Nb_2O_5 are depicted. Higher sintering temperature (group H) increases the number of pores and, in minor effect, its size. The morphology of the fracture surface (Figure 3 – 700 °C and Figure 4 – 800 °C) shows more pores at high temperatures. However, the specific mass is higher for the materials processed at 700 °C than 800 °C, indicating the vitrification of the surface processed at 800 °C that blocks water permeation.

The average biaxial flexural strengths are shown in Table 3. It is observed a reduction of the strength with increasing concentration of Nb_2O_5 at both temperatures. Moreover, the standard deviation reduces with the nucleating agent. This effect may be related to the intense crystallization of the specimens, with high contents of nucleating agents that produce more homogeneous materials. Furthermore, the Weibull modulus (m) of most groups is greater than 3. For fragile materials, the m parameter is considered acceptable in the range of 3-15, with the largest being the most reliable^{19,24}. The exception is the L15 group that presents a borderline value of 2.96 modulus. Although it is slightly lower than 3, this value is very close to the acceptable value. The determination factors R^2 , depicted in Table 3, are all greater than 0.88. According to work carried out by Defez et al.⁴⁷, R^2 values for flexural strength of ceramics greater than 0.80 are considered satisfactory. The equibiaxial mechanical test used here has advantages concerning the uniaxial test. Multiaxial stress states are required to evaluate failure theories applicable to component design and to assess samples with anisotropic flaw

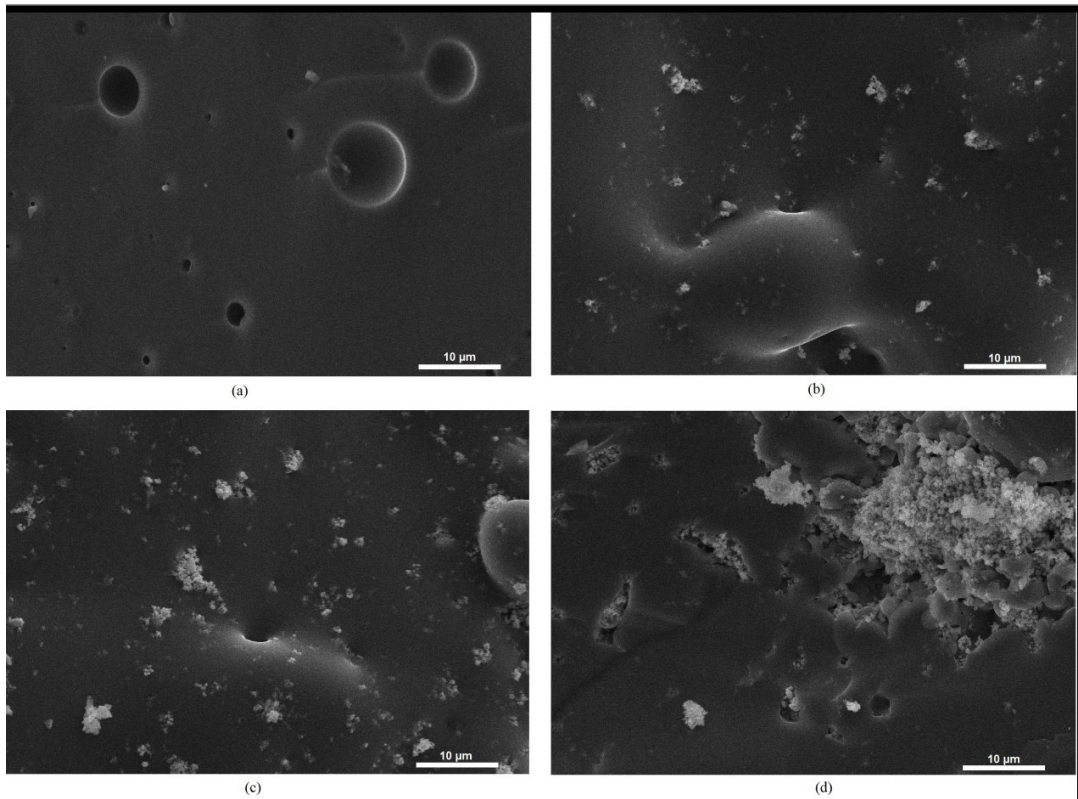


Figure 3. SEM photomicrographs of the glass-ceramic of the fracture surfaces of sintered samples at 700 °C: (a) 0, (b) 5, (c) 10, and (d) 15 wt% of Nb_2O_5 .

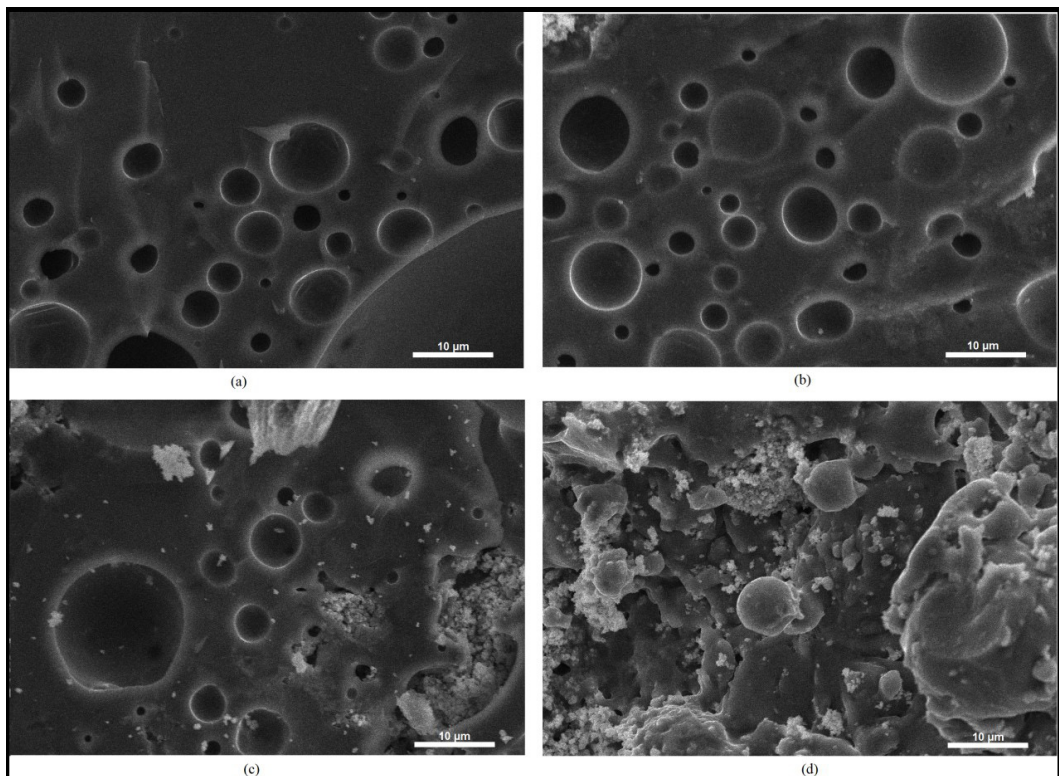


Figure 4. SEM photomicrographs of the glass-ceramic of the fracture surfaces of sintered samples at 800 °C: (a) 0, (b) 5, (c) 10, (d) 15 wt% of Nb_2O_5 .

distributions³⁸. Moreover, equibiaxial tests reduce the effects of specimen edge preparation as compared to uniaxial tests.

The Tukey test was used to compare post hoc all pairwise. An equal letter was termed for conditions without statistical significance ($p > 0.05$); otherwise, different letter shows means statistically significant ($p < 0.05$). At 700 °C, the strengths for L10 and L15 are similar (letter c). Without a nucleating agent (L0, letter a), this nucleating content produces a significantly higher mechanical strength than other pentoxide contents. L5 presents a significant strength value for a 0.05 confidence level. At a high temperature, 800 °C, the 5-15% content range does not produce a difference in the values, using the letter e. In other words, the addition of niobium pentoxide affects the mechanical behavior compared to without and with niobium pentoxide, but the higher temperature affects more than the nucleating amounts.

Porosity significantly affects the mechanical resistance, as shown in Figure 5. The porosity behavior is roughly the opposite of that observed for the resistance for each group. Pores have null mechanical resistance; thus, the biaxial strength reduces with porosity. Moreover, adding a nucleating agent increases porosity and reduces the resistance, regardless of the temperature. Even though the biaxial flexural strength values are not high, they are comparable with results of glass-ceramic composed of apatite and mullite crystals, glass-ceramic obtained from solid waste¹⁶, calcium phosphate cement, used in dentistry⁴⁸, as well as those of dental porcelain layers⁴⁹. The maximum strength is obtained for 0% niobium

pentoxide at 700 °C, with low porosity and a mean porous diameter of *ca.* 5 μm .

The electrical properties measured at the frequency of 1.0 kHz of glass-ceramic are shown in Table 4. The niobium pentoxide content and the sintering temperature affect the measured electrical properties in different ways. The most significant dielectric constants occurred for those glass-ceramics produced with 15 wt% of Nb_2O_5 content. The higher Nb_2O_5 concentration favors the increase of the dielectric constant due to the formation of the perovskite structure, NaNbO_3 . Niobium pentoxide promotes a solid-state reaction with glass powder, which contains sodium in its composition, forming sodium niobate above 550 °C⁴³. At 700 °C, the higher Nb_2O_5 concentration contents increase the dielectric constant, likely caused by the crystals of NaNbO_3 with only a perovskite structure. At 800 °C, the increase in the dielectric constant is smaller, probably because of the quartz phase. Thus, as observed by X-ray diffractograms, the produced glass-ceramics have two phases: perovskite sodium niobate and quartz. Due to the shape irregularities of some samples, the standard deviation of electrical parameters was relatively high concerning the mean, as for L5. This adverse effect is not found in very homogenous materials, such as metallic alloys. For ceramics, on the other hand, even with replicas, this dispersion can occur.

Niobates exhibit high dielectric constant, high polarization, and piezoelectric properties¹⁶. Thus, the monoclinic phase of NaNbO_3 with a perovskite structure was formed in

Table 3. Biaxial flexural strength, Weibull parameters, and Tukey analysis. Tukey test was applied to the averages within each temperature with a 0.05 confidence level. The superscripts with the same letter mean no statistical difference.

Group	Max stress (MPa)	Weibull modulus m	R ²
L0	34.83±10.32 ^a	3.25	0.96
L5	21.04±5.63 ^b	3.63	0.92
L10	14.67±3.27 ^c	4.44	0.92
L15	11.22±3.35 ^c	2.96	0.96
H0	28.66±7.59 ^d	3.63	0.88
H5	16.66±3.29 ^e	4.92	0.93
H10	13.80±2.27 ^e	6.14	0.98
H15	14.36±1.82 ^e	7.66	0.97

Tukey test was applied to the averages within each temperature with a 0.05 confidence level. The superscripts with the same letter mean no statistical difference.

Table 4. Electrical properties measured at 1.0 kHz.

Group	Dielectric constant	Dissipation factor (%)	Electrical conductivity ($\mu\text{S/m}$)	Capacitance (pF)
L0	9.4±0.5	14±9	0.1±0.09	8.3±0.5
L5	9.8±0.2	20±26	0.09±0.14	9.0±0.1
L10	11.8±0.6	10±2	0.07±0.02	11.4±0.4
L15	63.6±3.8	121±7	4.3±0.2	64±4
H0	7.8±0.5	25±12	0.10±0.07	5.2±0.5
H5	8.2±0.3	14±9	0.07±0.04	6.3±0.2
H10	8.9±0.4	17±9	0.09±0.05	7.9±0.3
H15	17.9±0.61	33±2	0.33±0.03	18.0±0.8

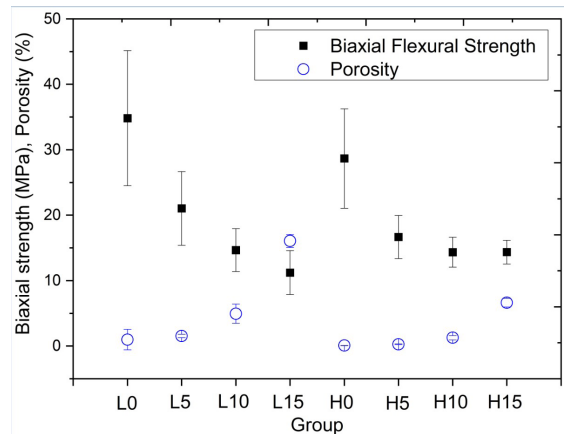


Figure 5. Biaxial flexural strength and porosity at 700 (L) and 800 °C (H) for 0, 5, 10, and 15 wt% Nb_2O_5 .

samples with the addition of niobium pentoxide. This phase supports the increase in dielectric constant for higher oxide concentration.

According to Yongsiri et al.⁵⁰, glasses may have a dielectric constant from 4.5 to 10. Without the addition of niobium pentoxide, the dielectric constant of glass-ceramic did not differ significantly from commercial glasses. However, with a small addition of niobium pentoxide, an increase in the dielectric constant is observed, reaching the highest value in the concentration of 15 wt%.

The formation of the crystalline perovskite structure reduces the ion content in the glass structure, decreasing the number of mobile charge carriers. Therefore, the electric conductivity reduces up to 10 wt%. Nonetheless, for 15 wt% at 700 °C, the electrical conductivity is higher and likely is related to the high dielectric constant. Shanker et al. (2009)⁵¹ reported a constant dielectric of 209 for pure NaNbO₃ measured at room temperature and 1.0 kHz. For condition H15 (15% Nb₂O₅ and 800 °C), the dielectric constant is approximately 18, and for L15 (15% Nb₂O₅ and 700 °C) is approximately 64. At 800 °C, the quartz is present in a high amount, as shown in the XRD peaks of Figure 2. Quartz has a low dielectric constant, around 3.8, which lowers the glass-ceramic constant. Dissipation factor represents the relative energy expenditure to storage a certain amount of energy, such as the d.c. Ohmic conductivity or a dissipation due to rotation of dipoles⁵². Although the relative quantity of phases, neither their morphology, were determined, these aspects likely reduce the efficiency of capacitors and increase the electrical conductivity.

As seen in x-ray diffraction, the addition of a nucleating agent promoted the formation of the crystalline structure of sodium niobate. In Singh et al.³³ paper, this structure showed a dielectric constant of 20.7, measured at the same frequency as the present work. The glass-ceramic specimens produced with only glass powder or low agent content exhibit characteristics of insulating material. However, the specimens with higher niobium oxide content have electrical conductivity features that approach the semiconductor range ($10^0 < \sigma_{el} < 10^{10} \mu\text{S}\cdot\text{m}^{-1}$)⁵⁴, with the sample L15 within this extensive range covering ten orders of magnitude typical for semiconductors. Furthermore, the dielectric constant augments strongly with the addition of 15 wt% of Nb₂O₅, likely caused by the greater quantity of crystals with perovskite structure. Thus, a higher dielectric constant occurs in specimens with 15 wt% of Nb₂O₅ than those that do not form sodium niobates or have a negligible amount.

Alkaline niobates, which include sodium niobate, have perovskite structures and semiconductive features. The Nb⁵⁺ ion induces ferroelectric behavior, which presents spontaneous polarization. The polarization promotes charge separation, created by the electronic transition from the valence band to the conduction band⁵⁵⁻⁵⁷. Alkaline sodium and potassium niobates, KNN, are a promising alternative to replace lead zirconate titanate, PZT, which has high lead content, highly harmful to the environment⁵⁸. However, although these alkaline niobates have excellent piezoelectric properties, their application is still limited by difficulties in their synthesis. One of the main challenges is to control the property reproducibility, usually associated with synthesis methods and sintering processes³³.

Thus, it becomes clear that materials containing alkaline niobates exhibit technological interest, and the production route with recycled glass powder and niobium pentoxide presented here may be a promising route.

Higher sintering temperatures did not increase the dielectric constant, despite facilitating crystallization. This behavior is affected by the greater porosity⁵⁹ or by the formation of two crystalline phases, decreasing the amount of the sodium niobate crystals. The higher electrical conductivities are also related to a higher percentage of niobium pentoxide. The highest electrical conductivity, 4.3 $\mu\text{S}/\text{m}$, is observed at 700 °C with 15 wt% of Nb₂O₅. Some glass-ceramics produced have electrical conductivity similar to semiconductor materials widely used for photocatalysis^{33,54}. For example, silicon carbide, a semiconductor, can have electrical conductivity in the range of 5-10 $\mu\text{S}/\text{m}$ ⁶⁰, comparable to the obtained results.

4. Conclusion

The obtained results show that using recycled glass powder from automotive windshields is possible to produce glass-ceramic. This glass-ceramic could be applied in electric devices, besides the reduction use of mineral resources from nature. The conclusions of the paper are:

- i) The addition of Nb₂O₅ allowed crystallization to occur at 700 °C, which does not occur with pure windshield glass powder. Increasing the sintering temperature to 800 °C promotes crystallization regardless of the addition of a nucleating agent.
- ii) A higher concentration of niobium oxide produces the monoclinic NaNbO₃ crystals at 700 °C; however, when sintered at 800 °C, two crystalline phases (monoclinic sodium niobite and quartz) are formed.
- iii) The sintering temperature and the Nb₂O₅ contents influence significantly the electric parameters but do not affect the behavior uniformly.
- iv) Equibiaxial flexural test is adequate for ceramics with flaw distribution and revealed that Nb₂O₅ addition in the range 0-15 wt% reduces the strength. At 800 °C, Tukey statistical test reveals that the mechanical behavior can be classified simply as without or with niobium pentoxide. Moreover, the strength reduced with the porosity, which increased with the addition of niobium oxide. The maximum strength is obtained for 0% niobium pentoxide at 700 °C, with low porosity and a mean porous diameter of *ca.* 5 μm .

5. Acknowledgements

This work was supported by FAPERJ and CNPq. This study was financed in part by the Coordenação de Aperfeiçoamento de Pessoal de Nível Superior – Brasil (CAPES) – Finance Code 001.

6. References

1. International Organization of Motor Vehicle Manufacturers [homepage on the Internet]. Paris: International Organization of Motor Vehicle Manufacturers; c2021 [cited 2022 May 11]. Available from: <https://www.oica.net/production-statistics/>

2. Šooš L, Matuš M, Pokusová M, Čačko V, Bábics J. The recycling of waste laminated glass through decomposition technologies. *Recycling*. 2021;15:26.
3. Mayyas M, Pahlevani F, Handoko W, Sahajwalla V. Preliminary investigation on the thermal conversion of automotive shredder residue into value-added products: graphitic carbon and nanoceramics. *Waste Manag*. 2016;50:173-83.
4. Xi C, Zheng F, Xu J, Yang W, Peng Y, Li Y, et al. Preparation of glass-ceramic foams using extracted titanium tailing and glass waste as raw materials. *Constr Build Mater*. 2018;190:896-909.
5. Lu J, Li Y, Zou C, Liu Z, Wang C. Effect of sintering additives on the densification, crystallization and flexural strength of sintered glass-ceramics from waste granite powder. *Mater Chem Phys*. 2018;216:1-7.
6. Lu X, Li Y, Dai W, Cang D. Effect of composition and sintering process on mechanical properties of glass ceramics from solid waste. *Adv Appl Ceramics*. 2016;115(1):13-20.
7. Rawlings RD, Wu JP, Boccaccini AR. Glass-ceramics: their production from wastes—a review. *J Mater Sci*. 2006;41(3):733-61.
8. Fredericci C, Yoshimura HN, Molisani AL, Pinto MM, Cesar PF. Effect of temperature and heating rate on the sintering of leucite-based dental porcelains. *Ceram Int*. 2011;37(3):1073-8.
9. Costa FP, Morais CRS, Rodrigues AM. Sustainable glass-ceramic foams manufactured from waste glass bottles and bentonite. *Ceram Int*. 2020;46(11):17957-61.
10. Yan Z, Feng K, Tian J, Liu Y. Effect of high titanium blast furnace slag on preparing foam glass-ceramics for sound absorption. *J Porous Mater*. 2019;26(4):1209-15.
11. Savvilidou V, Kritikaki A, Stratakis A, Komnitsas K, Gidarakos E. Energy efficient production of glass-ceramics using photovoltaic (P/V) glass and lignite fly ash. *Waste Manag*. 2019;90:46-58.
12. Fuertes V, Cabrera MJ, Scores J, Muñoz D, Fernández JF, Enríquez E. Enhanced wear resistance of engineered glass-ceramic by nanostructured self-lubrication. *Mater Des*. 2019;168:107623.
13. Denry IL, Holloway JA, Nakkula RJ, Walters JD. Effect of niobium content on the microstructure and thermal properties of fluorapatite glass-ceramics. *J Biomed Mater Res B Appl Biomater*. 2005;74B(1):18-24.
14. Si W, Ding C. An investigation on crystallization property, thermodynamics and kinetics of wollastonite glass ceramics. *J Cent South Univ*. 2018;8(25):1888-94.
15. Cao J, Lu J, Jiang L, Wang Z. Sinterability, microstructure and compressive strength of porous glass-ceramics from metallurgical silicon slag and waste glass. *Ceram Int*. 2016;42(8):10079-84.
16. Yio MH, Xiao Y, Ji R, Russell M, Cheeseman C. Production of foamed glass-ceramics using furnace bottom ash and glass. *Ceram Int*. 2021;47(6):8697-706.
17. Zhang W, Liu H. A low cost route for fabrication of wollastonite glass-ceramics directly using soda-lime waste glass by reactive crystallization-sintering. *Ceram Int*. 2013;39(2):1943-9.
18. Kang J, Wang J, Cheng J, Yuan J, Hou Y, Qian S. Crystallization behavior and properties of CaO-MgO-Al₂O₃-SiO₂ glass-ceramics synthesized from granite wastes. *J Non-Cryst Solids*. 2017;457:111-5.
19. Fan C-S, Li K-C. Production of insulating glass ceramics from thin film transistor-liquid crystal display (TFT-LCD) waste glass and calcium fluoride sludge. *J Clean Prod*. 2013;57:335-41.
20. Hemati S, Hossain R, Sahajwalla V. Selective thermal transformation of automotive shredder residues into high-value nano silicon carbide. *Nanomaterials*. 2021;11(11):2781.
21. Bó GCS-D, Bó MD, Bernardin AM. Reuse of laminated glass waste in the manufacture of ceramic frits and glazes. *Mater Chem Phys*. 2021;257:123847.
22. Munhoz H, Faldini SB, Miranda LF, Masson TJ, Maeda CY, Zandonadi AR. Recycling of automotive laminated waste glass in ceramic. *MSF*. 2014;798:588-93.
23. Lu J, Cong X, Lu Z. Influence of magnesia on sinter-crystallization, phase composition and flexural strength of sintered glass-ceramics from waste materials. *Mater Chem Phys*. 2016;174:143-9.
24. Ren Q, Liu C, Liu T, Zhang Q, Zhang Y, Ouyang Y, et al. Influence of nucleating agents on crystallization and electrical properties of SiO₂-MgO-MgF₂-K₂O mica glass-ceramics. *Ceram Int*. 2021;47(18):25997-6009.
25. Khater GA. Influence of Cr₂O₃, LiF, CaF₂ and TiO₂ nucleants on the crystallization behavior and microstructure of glass-ceramics based on blast-furnace slag. *Ceram Int*. 2011;37(7):2193-9.
26. Zhao M, Gao J, Shi Y, Li B-W. Effect of niobium pentoxide (Nb₂O₅) on the microstructure and properties of the diopside glass-ceramics produced from Bayan Obo mine tailing. *J Aust Ceram Soc*. 2020;56(3):1079-87.
27. Ciceo RL, Todea M, Toloman D, Muresan-Pop M, Simon V. Structure-composition correlation in niobium containing borophosphate glasses. *J Non-Cryst Solids*. 2020;542:120102.
28. Hsu JY, Speyer RF. Crystallization of Li₂O·Al₂O₃·6SiO₂ glasses containing niobium pentoxide as nucleating dopant. *J Am Ceram Soc*. 1991;74(2):395-9.
29. Lopes JH, Magalhães A, Mazali IO, Bertran CA. Effect of niobium oxide on the structure and properties of melt-derived bioactive glasses. *J Am Ceram Soc*. 2014;97(12):3843-52.
30. Pillis MF, Oliveira MCL, Antunes RA. Surface chemistry and the corrosion behavior of magnetron sputtered niobium oxide films in sulfuric acid solution. *Appl Surf Sci*. 2018;462:344-52.
31. Kalisz M, Grobelny M, Mazur M, Zdrojek M, Wojcieszak D, Świniarski M, et al. Comparison of mechanical and corrosion properties of graphene monolayer on Ti–Al–V and nanometric Nb₂O₅ layer on Ti–Al–V alloy for dental implants applications. *Thin Solid Films*. 2015;589:356-63.
32. Kong F, Tao S, Qian B, Gao L. Multiwalled carbon nanotube-modified Nb₂O₅ with enhanced electrochemical performance for lithium-ion batteries. *Ceram Int*. 2018;44(18):23226-31.
33. Nico C, Monteiro T, Graça MPF. Niobium oxides and niobates physical properties: review and prospects. *Prog Mater Sci*. 2016;80:1-37.
34. Gualberto HR, Lopes RS, Silva F, Schnurr E, Poiate Jr E, Andrade MC. Influence of sintering temperature on mechanical properties of glass-ceramics produced with windshield waste. *Int J Chem Eng*. 2019;2019:1-8.
35. Civici N, Vataj E. Analysis of automotive glass of various brands using EDXRF spectrometry. *Rom Rep Phys*. 2013;65:1265-74.
36. Saint-Gobain [homepage on the Internet]. Courbevoie: Saint-Gobain; c2021 [cited 2022 May 11]. Available from: <https://www.saint-gobain-autover.com.br/vidro-automotivo>
37. Gualberto HR, Moraes IA, Andrade MC, Poiate EJ, Arruda F, Poiate IAVP. Recycling of windscreen glass for glass-ceramic production com 15% niobium oxide. In: *Proceeding of the 21st National Meeting of Computational Modeling*; 2018 Oct 8-11; Brazil. *Proceedings. Rio de Janeiro: Instituto Federal Fluminense*; 2018, p. 1-11.
38. ASTM International: American Society for Testing and Materials. *ASTM C1499-19: standard test method for monotonic equibiaxial flexural strength of advanced ceramics at ambient temperature*. West Conshohocken: ASTM; 2019.
39. Chen X, Chan AHC. Modelling impact fracture and fragmentation of laminated glass using the combined finite-discrete element method. *Int J Impact Eng*. 2018;112:15-29.
40. Silva FT, Zacché MAN, Amorim HS. Influence of different surface treatments on the fracture toughness of a commercial ZTA dental ceramic. *Mater Res*. 2007;10(1):63-8.
41. Sens MA, Ueti E. Verificação da exatidão e linearidade na medição de capacitância e fator de dissipação. In: *VIII Semetro*; 2009 Jun 17-19; Brazil. *Proceedings. João Pessoa: Sociedade Brasileira de Metrologia*; 2009, p. 1-8.

42. Rezvani M, Eftekhari-Yekta B, Solati-Hashjin M, Marghussian VK. Effect of Cr_2O_3 , Fe_2O_3 and TiO_2 nucleants on the crystallization. *Ceram Int.* 2005;31:75-80.
43. Morais LA, Adán C, Araujo AS, Guedes APMA, Marugán J. Synthesis, characterization, and photonic efficiency of novel photocatalytic niobium oxide materials. *Global Chall.* 2017;1(9):1700066.
44. Li W, Xia X, Zeng J, Zheng L, Li G. Significant differences in NaNbO_3 ceramics fabricated using Nb_2O_5 precursors with various crystal structures. *Ceram Int.* 2020;46(3):3759-66.
45. Zhang WY, Gao H, Xu Y. Sintering and reactive crystal growth of diopside–albite glass–ceramics from waste glass. *J Eur Ceram Soc.* 2011;31(9):1669-75.
46. RRUFF Project [homepage on the Internet]. Tucson: RRUFF Project; 2015 [cited 2022 May 11]. Available from: <https://ruff.info/quartz/display=default/R050125>
47. Defez B, Peris-Fajarnés G, Santiago V, Soria JM, Lluna E. Influence of the load application rate and the statistical model for brittle failure on the bending strength of extruded ceramic tiles. *Ceram Int.* 2013;39(3):3329-35.
48. Luo J, Ajaxon I, Ginebra MP, Engqvist H, Persson C. Compressive, diametral tensile and biaxial flexural strength of cutting-edge calcium phosphate cements. *J Mech Behav Biomed Mater.* 2016;60:617-27.
49. Sawada T, Wagner V, Schille C, Spintzyk S, Schweizer E, Geis-Gerstorfer J. Effect of slow-cooling protocol on biaxial flexural strengths of bilayered porcelain-ceria-stabilized zirconia/alumina nanocomposite (Ce-TZP/A) disks. *Dent Mater.* 2019;35(2):270-82.
50. Yongsiri P, Senanon W, Intawin P, Pengpat K. Dielectric properties and microstructural studies of Er_2O_3 doped potassium sodium niobate silicate glass-ceramics. *Key Eng Mater.* 2018;766:258-63.
51. Shanker V, Samal SL, Pradhan GK, Narayana C, Ganguli AK. Nanocrystalline NaNbO_3 and NaTaO_3 : Rietveld studies, Raman spectroscopy and dielectric properties. *Solid State Sci.* 2009;11(2):562-9.
52. Hench LL, West JK. Principles of electronic ceramics. New York: John Wiley & Sons; 1990.
53. Singh K, Lingwal V, Bhatt SC, Panwar NS, Semwal BS. Dielectric properties of potassium sodium niobate mixed system. *Mater Res Bull.* 2001;36(13-14):2365-74.
54. Callister WD. Materials science and engineering: an introduction. 7th ed. New Delhi: Wiley; 2006.
55. Liu X, Qin C, Cao L, Feng Y, Huang Y, Qin L, et al. A silver niobate photocatalyst $\text{AgNb}_7\text{O}_{18}$ with perovskite-like structure. *J Alloys Compd.* 2017;724:381-8.
56. Hong Y, Li J, Wu W, Wu Y, Bai H, Shi K, et al. Structure, electricity, and bandgap modulation in Fe_2O_3 -doped potassium sodium niobate ceramics. *Ceram Int.* 2018;44(13):16069-75.
57. Barbosa-Silva R, Silva JF, Rocha U, Jacinto C, Araújo CB. Second-order nonlinearity of NaNbO_3 nanocrystals with orthorhombic crystalline structure. *J Lumin.* 2019;211:121-6.
58. Yang D, Yang Z, Zhang X, Wei L, Chao X, Yang Z. High transmittance in lead-free lanthanum modified potassium-sodium niobate ceramics. *J Alloys Compd.* 2017;716:21-9.
59. Zeng T, Dong X, Mao C, Zhou Z, Yang H. Effects of pore shape and porosity on the properties of porous PZT 95/5 ceramics. *J Eur Ceram Soc.* 2007;27(4):2025-9.
60. Kim Y-W, Kim Y-H, Kim KJ. Electrical properties of liquid-phase sintered silicon carbide ceramics: a review. *Crit Rev Solid State Mater Sci.* 2020;45(1):66-84.